J. Fluid Mech. (1972), *vol.* 53, *part* 1, *pp.* 61–83
Printed in Great Britain

Large-scale motion of a turbulent boundary layer during relaminarization

By RON F. BLACKWELDER† AND LESLIE S. G. KOVASZNAY
Department of Mechanics, The Johns Hopkins University

(Received 8 June 1971)

A fully developed turbulent boundary layer was subjected to a strongly favourable pressure gradient in order to investigate the role of the large eddy structure during 'relaminarization'. Measurements of the mean velocity profiles indicated that the 'law of the wall' disappeared in the region of the maximum pressure gradient. The three fluctuating velocity components and the tangential Reynolds stress were obtained to determine more precisely the nature of the decay of the turbulent structure. These measurements indicated that the absolute level of the velocities and stress were approximately constant along a mean streamline except near the wall. However, the relative levels were decreasing, as reported previously by several authors. The intermittency factor γ decreased along the mean streamlines until most of the boundary layer had only a negligible turbulence level. Space–time auto- and cross-correlations of u, v and I (the intermittency function) of the large-scale structure were obtained in the region of maximum pressure gradient and are compared with those measured in a zero pressure gradient flow.

1. Introduction

The curious fact that a turbulent boundary layer reverts towards a laminar state when undergoing a rapid acceleration through a strongly favourable pressure gradient was first noticed by Sternberg (1954) in supersonic flow. Since then several investigators have sought to explore this process in more detail. Kline *et al.* (1967) noticed that the violent outward eruptions away from the wall near the edge of the viscous sublayer ceased when the pressure gradient reached a critical value given by

$$\frac{-\nu}{U^3\rho}\frac{dP}{dx} = 3{\cdot}7 \times 10^{-6}.$$

Badri Narayanan & Ramjee (1968) stated that the process of relaminarization is more closely associated with a decreased Reynolds number based on the momentum thickness than with the pressure gradient. Fiedler & Head (1966) have shown that the intermittency pattern becomes wider and that the half-intermittency point moves closer to the wall in a favourable pressure gradient.

† Present address: Department of Aerospace Engineering, University of Southern California, Los Angeles.

They speculated that relaminarization occurs when the intermittency pattern occupies the whole boundary layer, thus giving a laminar-like flow with some isolated turbulent patches that are presumably in a state of decay.

The phenomenon of relaminarization is not confined to a turbulent boundary layer. In three different turbulent flows, a pipe, channel and boundary layer, Patel & Head (1968) studied the earlier stages of relaminarization by measuring mean quantities and determining the location of the disappearance of the 'law of the wall'. They found the process of relaminarization to be independent of Reynolds number and suggest that it depends only upon a parameter involving the shear-stress gradient in the wall region. In another investigation, Badri Narayanan (1968) studied reverse transition in a channel and found that the mean velocity profile became more parabolic and that the turbulence levels and production of turbulent energy decreased. In addition, Moretti & Kays (1965) and others have examined the convective heat-transfer rates of various flow fields undergoing relaminarization and have also obtained criteria for the initiation of this phenomenon.

The above studies have shown that under suitable conditions turbulent shear flows over solid boundaries can become more 'laminar-like'. It is obvious that the pressure gradient is not universally responsible for this phenomenon as the pressure gradient is favourable in the case of the boundary layer and adverse in channel flows. However, in all cases the relevant Reynolds number was reduced, the sublayer thickness increased and the mean velocity profile became more laminar-like.

2. Experimental equipment

All measurements were taken in a low-speed open-return wind tunnel. The power plant was a centrifugal blower, followed by a diffuser section and then a 420 cm wide, 360 cm high and 210 cm long settling chamber provided with seven fine mesh screens. After the settling chamber there was a two-dimensional contraction (7:1) in the horizontal plane, leading into a nearly parallel section upstream of the test section which allowed for the development and growth of the boundary layer. The width of this section was slightly flared in order to allow for the boundary-layer growth. It had a nominal width of 52 cm, a constant height of 360 cm and was 970 cm long. Following the parallel section, the pressure gradient was formed by a smooth two-dimensional contraction over the last 250 cm of the working section as shown in figure 1. This section reduced the width of the test section from 54 cm to 12 cm at the exit. Since the overall height of 360 cm was maintained, special care was taken in aligning the contour to ensure two-dimensionality. On each vertical wall at $x = 243$ cm a row of 0·3 cm high hemispherical head upholstery tacks, spaced 3·5 cm apart, tripped the boundary layer in order to obtain a well-established turbulent boundary layer. All the measurements were made on one wall, which was built to be plane within $\pm$ 0·0125 cm over the entire length and height of the tunnel.

The x co-ordinate is aligned with the free-stream velocity in the upstream parallel section, the y co-ordinate is perpendicular to the wall and z is the span-

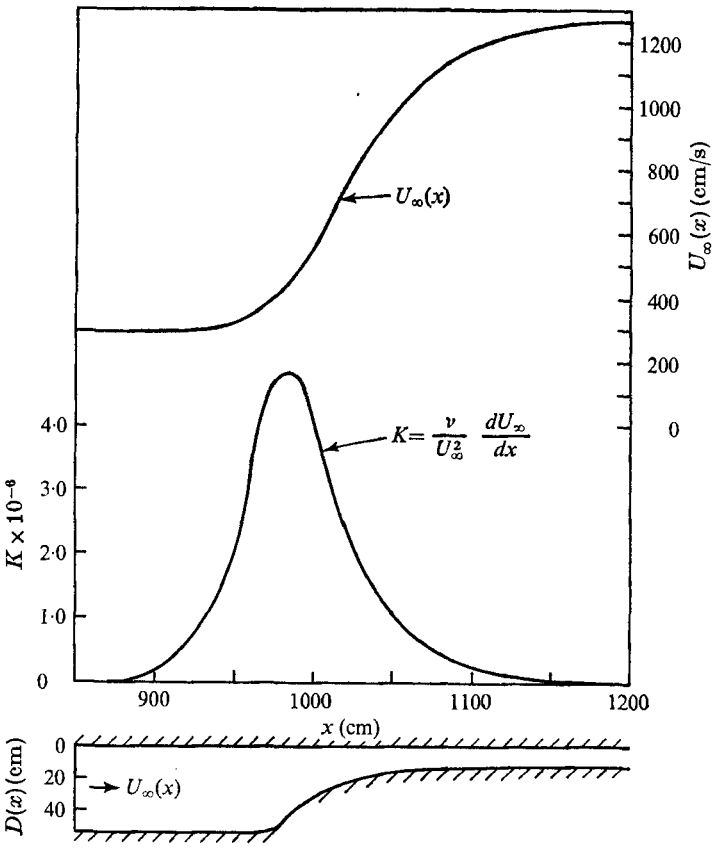

FIGURE 1. Shape of the contraction and the resulting velocity and pressure distributions.

wise co-ordinate. Traversing was continuous in all three co-ordinates with an accuracy of $\pm 0{\cdot}05$ cm in the x co-ordinate, $\pm 0{\cdot}003$ cm in the y co-ordinate and $\pm 0{\cdot}10$ cm in the z co-ordinate. The non-dimensional co-ordinates used in the correlation contours are

$$X = (x-x_0)/\delta_0, \quad Z = (z-z_0)/\delta_0, \quad T = U_0\tau/\delta_0,$$

where U_0 and δ_0 are the free-stream velocity and boundary-layer thickness at $x = 875$ cm and $\tau = t-t_0$ is the time delay.

An access window was constructed which could be placed at any streamwise position before and along the contraction section and which would assume the appropriate contour at that location. Owing to the large vertical dimension of the test section (360 cm) the traverse of the access window was limited to $130 < z < 230$ cm.

For relaminarization in a boundary layer, a critical value of the non-dimensional pressure gradient

$$K = \frac{-\nu}{\rho U_\infty^3}\frac{dP}{dx} = \frac{\nu}{U_\infty^2}\frac{dU_\infty}{dx}$$

must be obtained as reported by Kline *et al.* (1967) and Badri Narayanan & Ramjee (1968). The contraction used in this investigation was designed to attain the critical non-dimensional pressure gradient early in the test section, near $x = 975$ cm. The pressure gradient was then allowed to relax until the free stream was parallel again at the exit.

Constant-temperature hot-wire anemometers were used in the manner described by Kovasznay, Miller & Vasudeva (1963). Linearizers of the basic type designed by Kovasznay & Chevray (1969) were used after determining a different set of resistors in the transitor chain which were more appropriate to the velocities encountered in this investigation. The output voltages of the linearizers were set typically to 2·0 volts in the free stream. Each output voltage was then d.c. coupled to a Philbrick Model K2-W chopper stabilized amplifier for analog computation. The frequency response of the amplifiers was flat within $\pm 1{\cdot}0\,\%$ over 0–5000 Hz. The multiplier used to obtain the Reynolds stress was a G.P.S. Model MU 407 Analog Multiplier, which had a flat response ($\pm 1{\cdot}0\,\%$) over the frequency range 0–50 kHz with an accuracy of $\pm 0{\cdot}5\,\%$ of full-scale amplitude.

In the accelerated flow it was desirable to obtain data as close to the wall as possible. This presented no problem for the streamwise velocity component u, for which a single wire could be aligned in the spanwise direction and could be traversed in increments of 0·003 cm towards the wall. However, for the v and w velocity components a special X-probe was constructed using a welding technique to attach the wires to the brooches in order to minimize the lateral dimension of the probe. In this case, bare tungsten wires 3·8 μm in diameter and 0·20 cm long were welded directly to the jeweller's brooches tapered to 0·008 cm diameter at the tip. The wires were 0·02 cm apart and were inclined approximately at 45° to the x axis, so the total width of the probe was only 0·14 cm. The X-probe was calibrated by a direct yawing procedure in the free stream.

When measuring the normal velocity fluctuations and the Reynolds stress, the wires of the X-probe were aligned in the x, y plane, so that near the wall the wires experience a large mean velocity gradient along their length. Since there is no acceptable method of determining how much error this velocity gradient introduces into the measurements, the criterion used here was that the data were accepted and presented as long as the $\overline{U}$ and u' measurements obtained from the X-probe agreed with the measurements obtained from a single wire aligned in the spanwise direction.

Probe interference was minimized in the space–time correlation data by inclining the upstream probe axis at 45° to the free-stream velocity vector in the x, z plane. Four needles extended 2·5 cm outward from the main body of the probe and their tips lay in the x, y plane. Two copper-plated 3·8 μm tungsten wires with a 0·20 cm sensitive region were soft soldered to the needles. Some probe interference was still apparent at $z = 0$, hence those correlation values were obtained by extrapolation as $Z \to 0$.

The turbulence detector probe consisted of two hot wires aligned in the spanwise direction and separated by a distance d. The signal difference between the two hot-wire outputs was used by the turbulence detector described by Kovasznay, Kibens & Blackwelder (1970) to decide whether the fluid at the

detector probe's location was turbulent or non-turbulent. Since the decision criteria depend upon the relation of d to the spatial scales of the turbulence, d was always set to be $\frac{1}{2}\lambda$, where λ is Taylor's microscale.

In the region of the accelerated flow where the new turbulence was generated a single wire detector probe was used to obtain the intermittency function $I(t)$, because the distinction between the old decaying turbulence and the new turbulence was extremely sharp. The output of the detector gave $I(t-\tau_h)$, namely the intermittency function $I(t)$ delayed by τ_h, the 'hold time' of the detector. When measuring the cross-correlation of $I(t)$ and another flow variable (u or v), τ_h was added to (or subtracted from) the time delay read on the correlator. The random square wave $I(t)$ was used to modulate a pulse train of typically $f_P = 2\,\text{kHz}$. By counting the pulses during a fixed time interval (typically 50 s) the intermittency factor γ was read directly on an electric counter. The electronic counter was a Model 6144 Universal EPUT and Timer manufactured by Beckman Instruments Inc.

The space–time correlations were obtained by a Correlation Function Computer, Model 101A, manufactured by Princeton Applied Research, Princeton. The computational accuracy is 2 % of the maximum correlation and an additional 3 % error occurs at very low correlation levels because of internal noise. The time delay accuracy is 0·5 % of the maximum time delay.

3. Experimental results

3.1. *Mean flow*

The wind tunnel configuration used is shown to scale in figure 1 along with the resulting velocity and pressure distributions. The velocity increased from 295 to 1260 cm/s. The acceleration of the flow is expressed by the non-dimensional pressure gradient

$$K = -\frac{\nu}{\rho U_\infty^3}\frac{dP}{dx} = \frac{\nu}{U_\infty^2}\frac{dU_\infty}{dx}. \tag{1}$$

As shown in figure 1, it reaches a maximum value of $4{\cdot}8 \times 10^{-6}$ at $x = 984\,\text{cm}$ and then decreases to zero at the exit.

Initial measurements indicated that the mean flow distribution was tending toward a laminar boundary layer in the region $970 < x < 1070\,\text{cm}$. After the pressure gradient had relaxed considerably, new turbulent spots began appearing close to the wall;

$$8 < yu_*/\nu < 30 \quad \text{at} \quad x = 1070\,\text{cm}.$$

At the exit, $x = 1200\,\text{cm}$, the boundary layer was again fully turbulent. Since the essential features of the desired flow were obtained in the highly accelerated region, the fact that new turbulence erupted further downstream caused little concern.

The variations of the displacement thickness $\delta^*(x)$ and the momentum thickness $\theta(x)$ are given in figure 2. The pressure gradient is so severe that both these integral parameters are reduced by more than a factor of ten. In the relaxation region beyond $x = 1070\,\text{cm}$, these parameters increase slightly as the new turbulent boundary layer grows downstream.

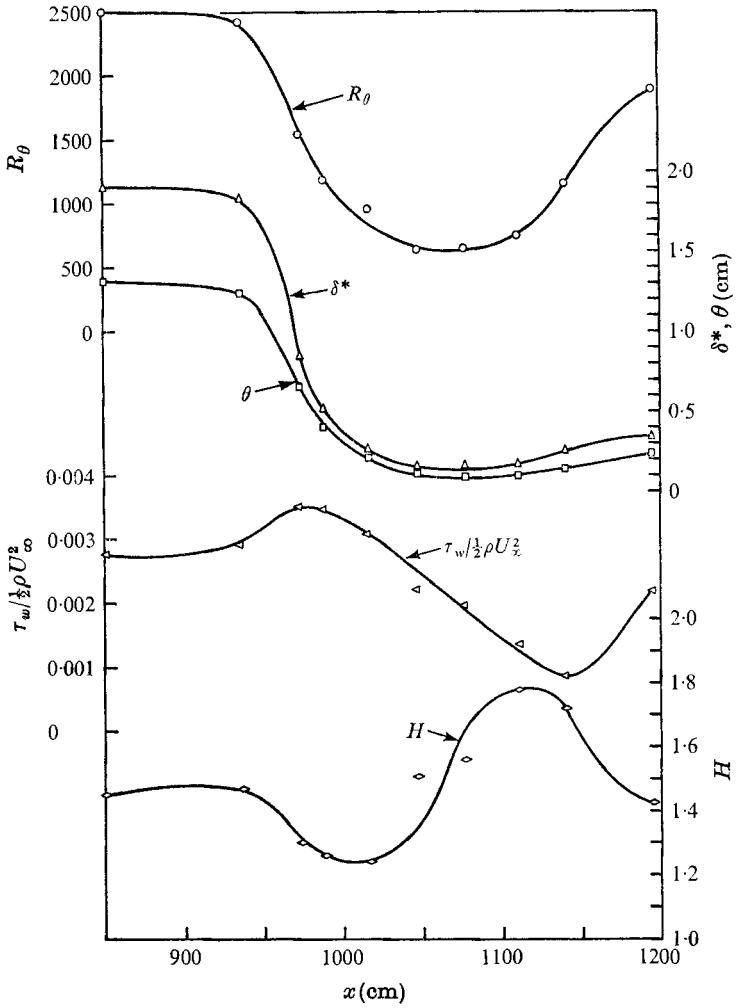

FIGURE 2. Distribution of the Reynolds number $U_\infty \theta/\nu$, displacement thickness, momentum thickness, wall shearing stress and shape parameter in the accelerated flow.

The Reynolds number based upon the momentum thickness, R_θ, and the shape parameter $H = \delta^*/\theta$ are also shown in figure 2. The Reynolds number decreases from a value of 2500 upstream to approximately 650 at $x = 1070$ cm. Then it increases again as the new turbulent boundary layer grows and reaches a final value of 1900 at the exit. The shape factor decreases as the boundary layer enters the favourable pressure gradient and reaches a minimum value of approximately 1·24, which agrees with the minimum values found by Fiedler & Head (1966) in boundary layers undergoing relaminarization. The shape factor increases in the region $1000 < x < 1110$ cm as the layer becomes more 'laminar-like'. Further downstream the new turbulence reduces the shape factor again to the value of that in a zero pressure gradient turbulent boundary layer.

The distribution of the non-dimensional shear stress was obtained by measuring the velocity gradient in the viscous sublayer near the wall and is shown in figure 2.

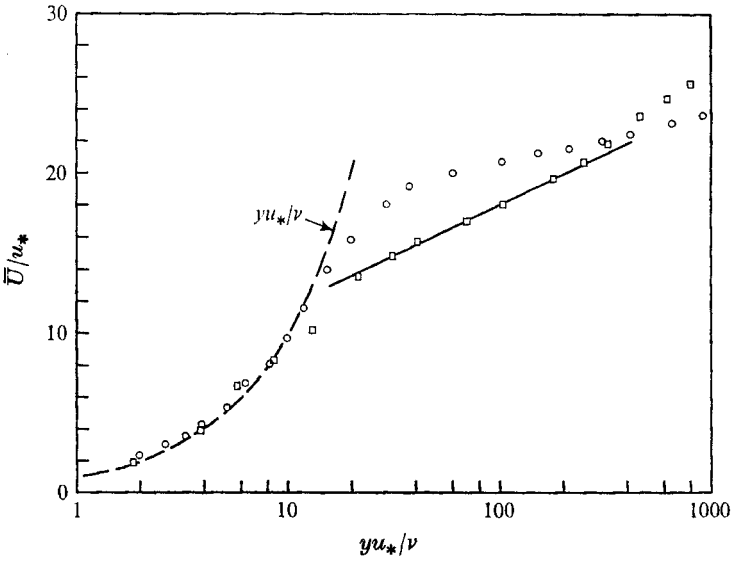

FIGURE 3. Departure from the logarithmic 'law of the wall' in the accelerated flow. □, $x = 936$ cm; ○, $x = 990$ cm.

The observed initial rise is similar to that reported by Badri Narayanan & Ramjee (1968). The shear stress at the wall then begins to decrease towards its laminar value but the new turbulence again causes an ultimate increase. However, the shearing stress at the wall does not begin to increase until approximately 70 cm downstream from the appearance of the new turbulent spots, in contrast to the immediate effect of the new turbulence on the other parameters.

In a strongly favourable pressure gradient, Badri Narayanan & Ramjee (1968) and Patel & Head (1968) have found that the logarithmic 'law of the wall' is no longer valid. In the present investigation the logarithmic region disappeared in the region of maximum acceleration between $x = 936$ and 990 cm as shown in figure 3. At $x = 936$ cm, a logarithmic region extending over one decade in y^+ was found with a corresponding friction velocity of $u_*/U_\infty = 0{\cdot}0385$ determined by the slope. This value agrees quite well with the value

$$u_*/U_\infty = (\tau_w/\rho U_\infty^2)^{\frac{1}{2}} = 0{\cdot}0381$$

obtained from figure 2 at $x = 936$ cm. However, at $x = 990$ cm the logarithmic region has disappeared and the mean velocity profile near the wall resembles a laminar layer. At $x = 1067$ cm the mean velocity data followed a linear profile to an even larger value of y^+.

The present investigation was mainly concerned with observing the decay of the turbulent structure in the rapidly accelerating flow. In order to visualize the variation of the turbulent parameters at different x stations it was decided to characterize the distance from the wall by the stream function ψ instead of by y, where

$$\frac{\psi(x,y)}{\nu} = \frac{1}{\nu}\int_0^y \bar{U}(x,y')\,dy'. \tag{2}$$

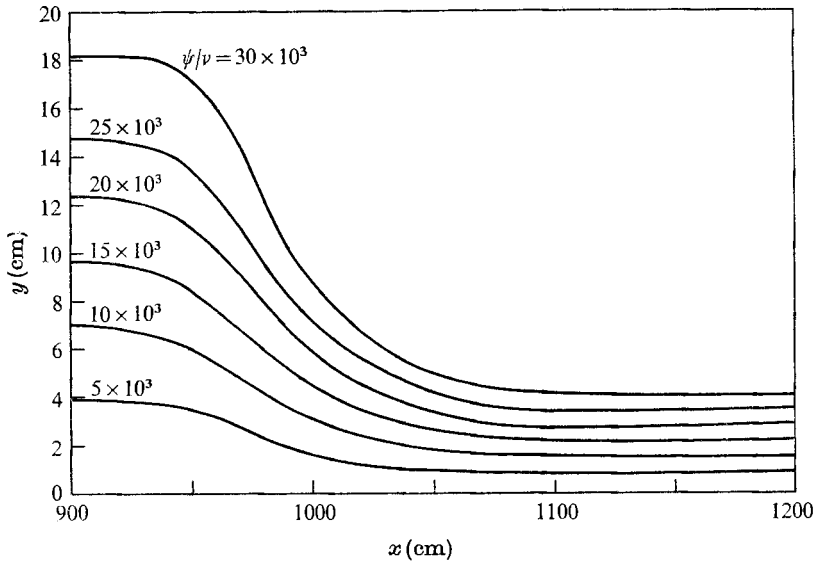

FIGURE 4. Mean streamlines and stream function in the favourable pressure gradient flow.

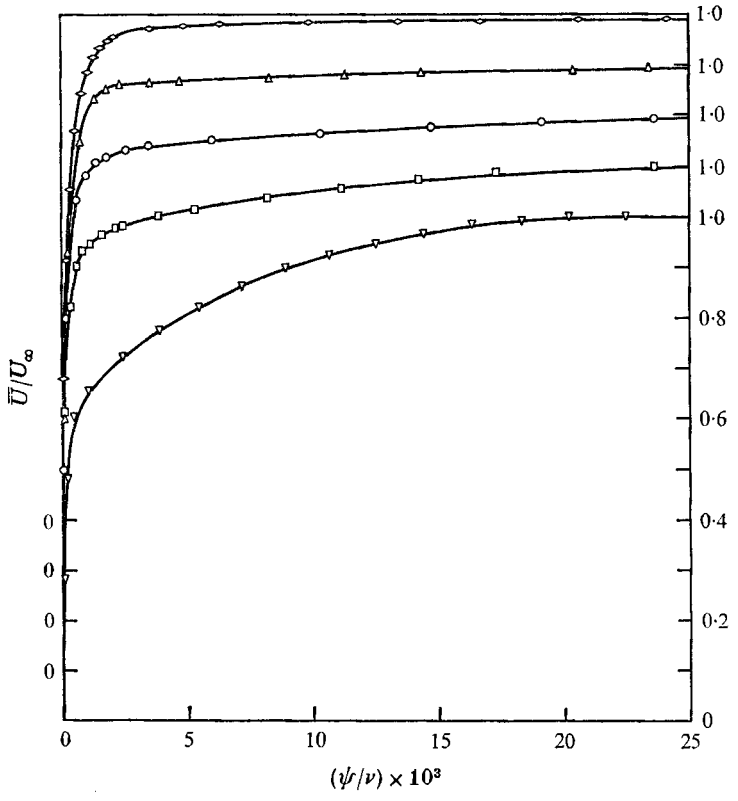

FIGURE 5. Mean velocity profiles in the accelerated flow. Note the displaced origin for each x station. ▽, $x = 936$ cm; □, $x = 988$; ○, $x = 1016$; △, $x = 1047$; ◇, $x = 1077$.

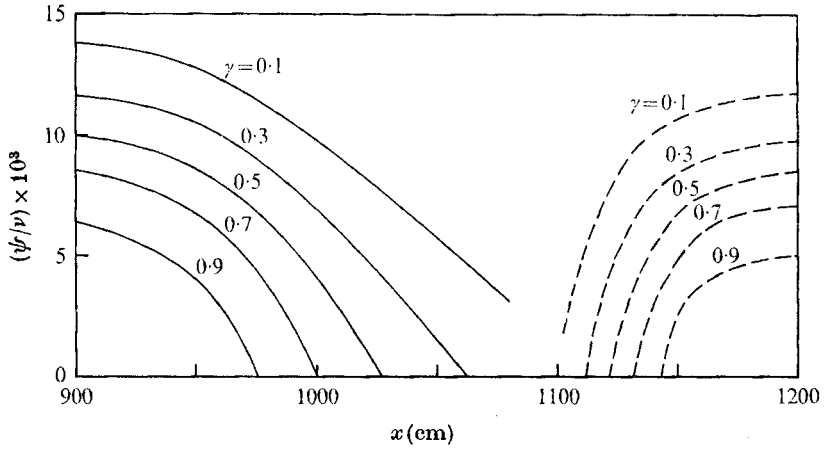

FIGURE 6. Variation of the intermittency factor in the accelerated boundary layer.

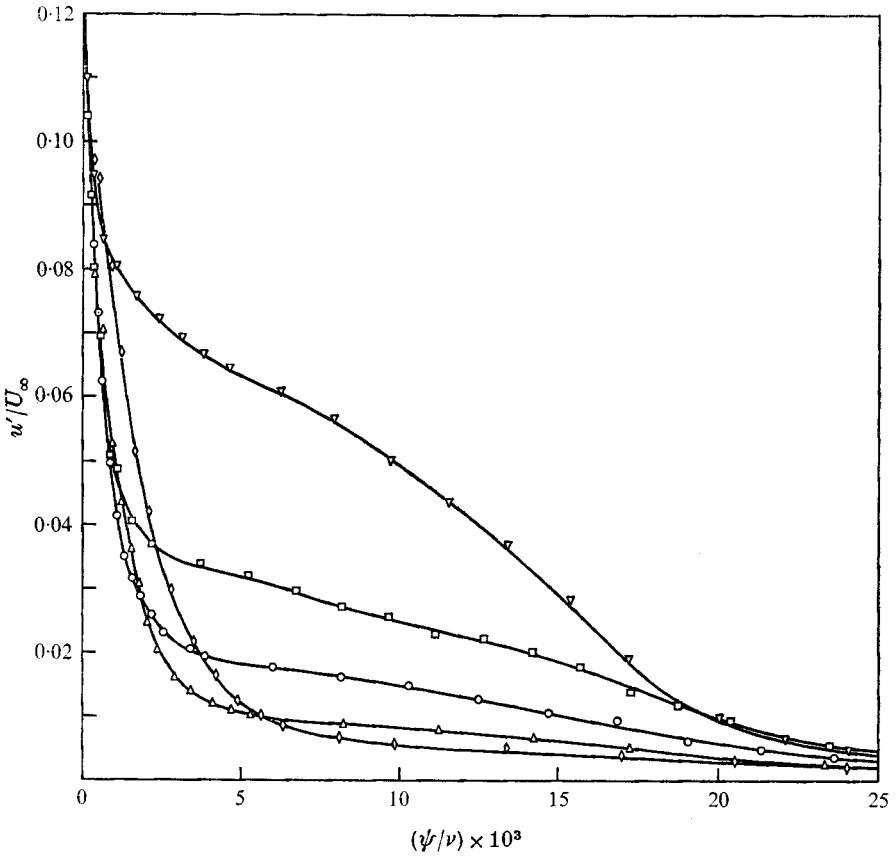

FIGURE 7. Intensities of the streamwise velocity component in the accelerated flow. ▽, $x = 936$ cm; □, $x = 988$; ○, $x = 1016$; △, $x = 1047$; ◇, $x = 1077$.

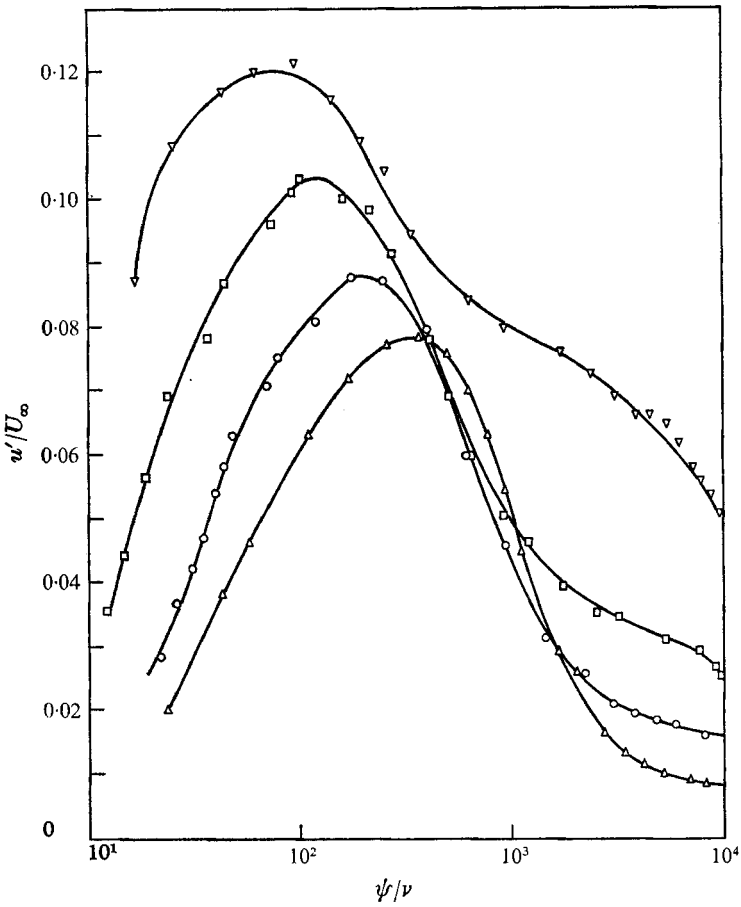

FIGURE 8. Intensities of the streamwise velocity component in the accelerated flow near the wall. ▽, $x = 936$ cm; □, $x = 988$; ○, $x = 1016$; △, $x = 1047$.

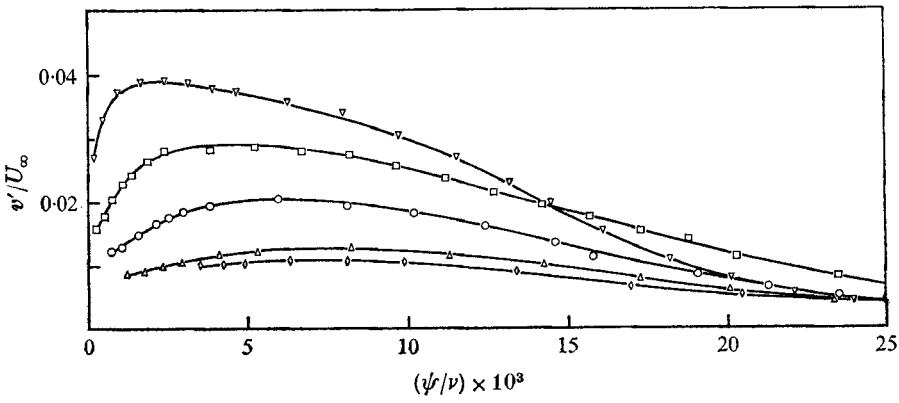

FIGURE 9. Intensities of the normal velocity component in the accelerated flow. ▽, $x = 936$ cm; □, $x = 988$; ○, $x = 1016$; △, $x = 1047$; ◇, $x = 1077$.

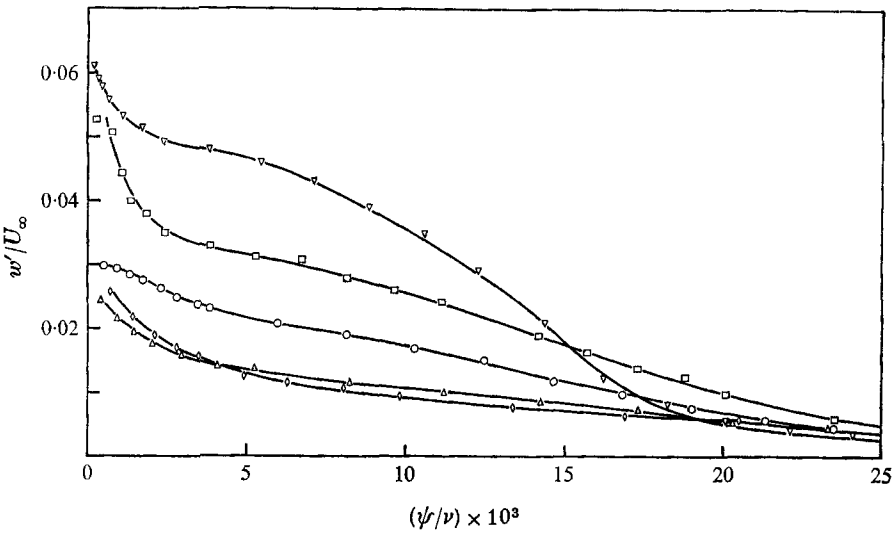

FIGURE 10. Intensities of the transverse velocity component in the accelerated flow. ▽, $x = 936$ cm; □, $x = 988$; ○, $x = 1016$; △, $x = 1047$; ◇, $x = 1077$.

In this manner the development of the turbulent parameters along the mean streamlines could be determined more conveniently. The calculated stream function and the mean streamlines are shown in figure 4.

The mean velocity profiles are shown in figure 5. Note the staggered origins for the ordinate of each curve. The rapid acceleration has substantially increased the thickness of the viscous sublayer and has considerably reduced the velocity defect in the outer regions. Similar results were reported by Patel & Head (1968).

3.2. *Intermittency factor*

Fiedler & Head (1966) have shown that in an accelerated boundary layer the intermittent region gradually occupies the entire thickness of the layer. The intermittency measurements reported here show similar results (see figure 6). Not only did the constant intermittency contours move towards the wall when expressed in terms of the absolute distance y, but they also moved inward across the mean streamlines. That is, along any mean streamline through the strongly favourable pressure gradient, the intermittency factor decreases continuously. The intermittency factor measured in the newly formed turbulence is given by the dashed lines.

3.3. *Turbulent intensities and energy*

The fluctuation levels of the streamwise velocity component, $u'/U_\infty(x)$, are shown in figures 7 and 8. In the outer region of the boundary layer the intensity is decaying along the mean streamlines (see figure 7), although most of this decay is caused by the increase in the free-stream velocity $U_\infty(x)$, used for normalization. The absolute values of the fluctuation level remain approximately constant along a mean streamline. The same quantity nearer the wall is shown in figure 8; the

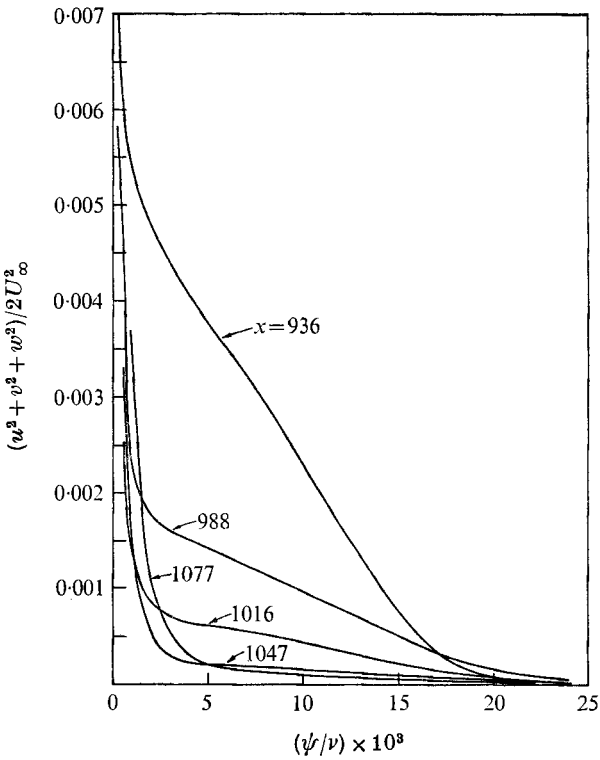

FIGURE 11. Distribution of the energy of the velocity fluctuations in the accelerated flow.

maximum value decreases from 0·12 to 0·079 and the location of the maximum moves outwards from the wall.

The intensities of the other two velocity components are shown in figures 9 and 10. Both decrease along the mean streamlines when normalized with the local free-stream velocity $U_\infty(x)$, but again the absolute values of these fluctuating intensities in the outer region remain almost constant. One interesting feature of all three turbulent intensities is that they show a slight increase in the outer region of the boundary layer; i.e. for $\psi/\nu \gtrsim 20\times 10^3$ there is a slight increase in the intensities as the flow is accelerated.

The total kinetic energy of the velocity fluctuations normalized with $U_\infty(x)$ is presented in figure 11. The energy decays along the streamlines in the relaxing region until the new turbulence appears. Most of the decay is only relative because $U_\infty(x)$ increases rapidly along the flow, thus reducing the normalized values. In figure 12 the absolute value of the kinetic energy of the velocity fluctuation is shown normalized with U_0, the free-stream velocity in the upstream constant pressure flow ($U_0 = 295$ cm/s). Using this method, the data collapse considerably which shows that along each mean streamline there is very little decay of the absolute energy. An interesting aspect of figure 12 is that in the outer part of the layer, $\psi/\nu \gtrsim 15\times 10^3$, the absolute value of the energy actually increases.

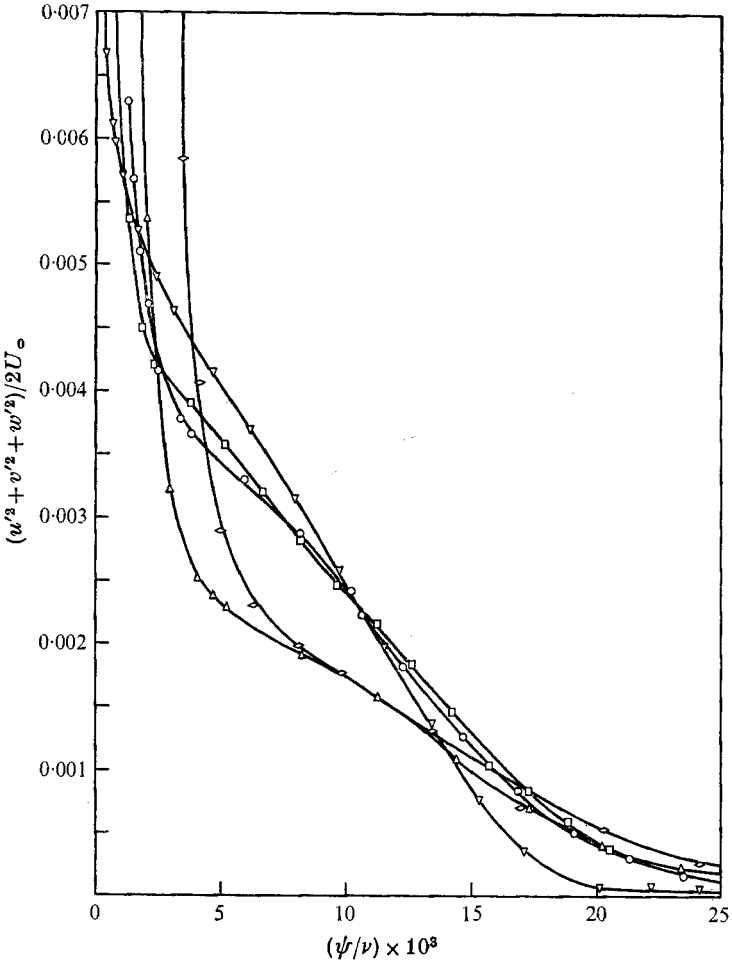

FIGURE 12. Distribution of the absolute energy of the velocity fluctuations in the accelerated flow. ▽, $x = 936$ cm; □, $x = 988$; ○, $x = 1016$; △, $x = 1047$; ◇, $x = 1077$.

This is unexpected since it is usually assumed that in the free stream of any nozzle the turbulent kinetic energy will decrease.

3.4. *Reynolds stress*

The tangential Reynolds stress $\overline{uv}/U_\infty^2$ was measured at the same stations (except $x = 1047$ cm) in the accelerated flow and is shown in figure 13. For $\psi/\nu \gtrsim 15 \times 10^3$, there is always a decrease along each streamline going downstream. On the other hand, for $\psi/\nu \lesssim 15 \times 10^3$ there is a general increase in the Reynolds stress above its unaccelerated value.

The absolute value of the Reynolds stress was also calculated by normalizing with U_0 instead of $U_\infty(x)$ and is shown in figure 14. Immediately after the flow begins to accelerate there is an increase in the absolute value of the absolute Reynolds stress all across the layer, but shortly after this initial increase there

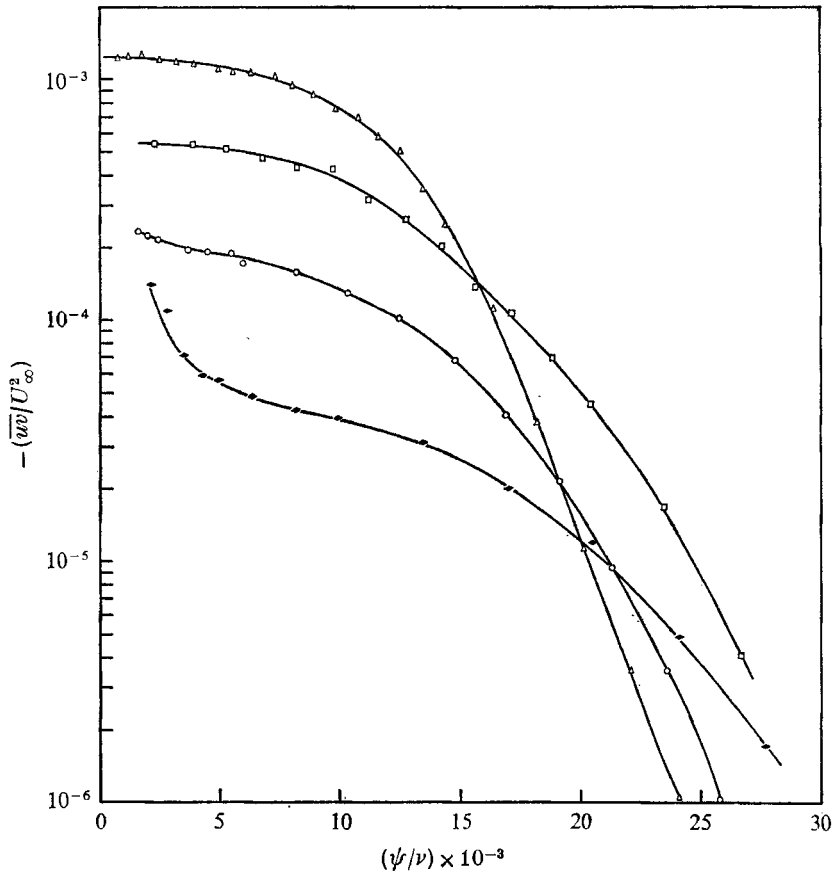

FIGURE 13. Variation of the Reynolds stress in the accelerated flow. △, $x = 936$ cm; □, $x = 988$; ○, $x = 1016$; ◇, $x = 1077$.

is a general decrease. The absolute level of the Reynolds stress in the outer regions, $\psi/\nu \lesssim 15 \times 10^3$, always remains greater than its original value in the unaccelerated flow. In the relaxing region at $x \geqslant 1070$ cm the new turbulence being generated near the wall sharply increases the Reynolds stress there. Even though the Reynolds stress has increased slightly in the outer regions, the production of turbulent energy remains quite small there because $\partial \overline{U}/\partial y$ is quite small.

When comparing figures 13 and 14 with figure 8 it appears that there is a small but significant Reynolds stress $\overline{uv}$ present in the non-turbulent region. This is not surprising in view of Stewart's (1956) analysis, which suggests that there is a Reynolds stress gradient perpendicular to the plane of a two-dimensional turbulent wake in order to balance the gradient of the turbulent intensities in the streamwise direction. Presumably the same type of analysis may be applied to the present streamwise inhomogeneous case, yielding similar results.

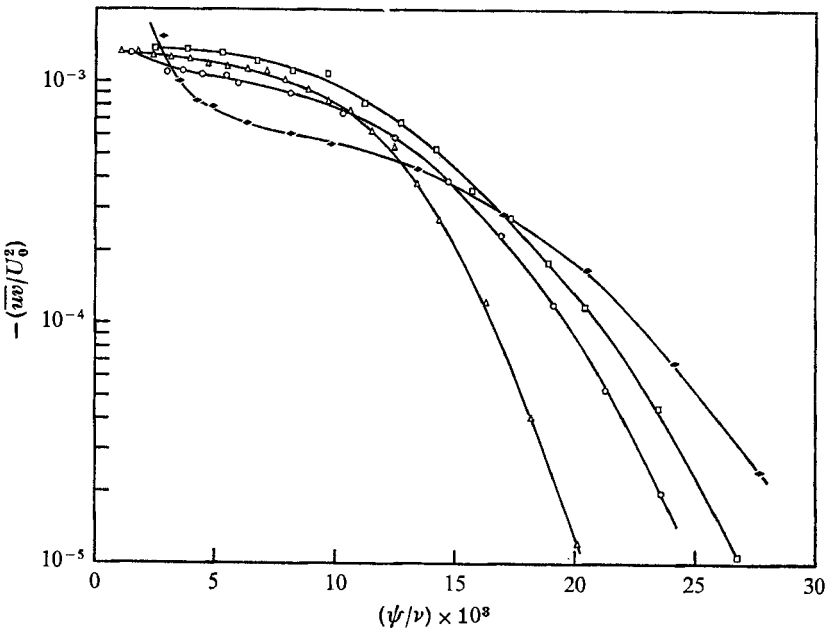

FIGURE 14. Variation of the absolute value of the Reynolds stress in the accelerated flow. △, $x = 936$ cm; □, $x = 988$; ○, $x = 1016$; ◇, $x = 1077$.

3.5. *Space–time correlations*

The space–time correlations in the pressure gradient were taken in such a way that the absolute time delay was the same as in the zero pressure gradient flow reported by Kovasznay, Kibens & Blackwelder (1970). In this manner the influence of the acceleration can be seen more clearly because the time scale of the eddy decay must be approximately the same in both cases.

For a fluid particle travelling along a fixed streamline $\psi = \psi_1$, the time required to travel a distance dx in the accelerated flow is

$$d\tau = dx/U(x, \psi_1), \quad \psi_1 = \text{constant}.$$

For a given spatial separation $x - x_0$ the maximum correlation is expected to appear near

$$\tau_{\max} = \int_{x_0}^{x} \frac{dx'}{U(x', \psi_1)}, \quad \psi_1 = \text{constant}.$$

The spatial separation $x - x_0$ was determined so that the non-dimensional time delay for maximum correlation

$$T_{\max} = U_0 \tau_{\max}/\delta_0$$

would be the same for both the zero and favourable pressure gradient flows. In the accelerated case, U_0 and δ_0 are the free-stream velocity and boundary-layer thickness at the end of the zero pressure gradient flow at $x = 875$ cm. In the unaccelerated flow U_0 and δ_0 are the local values of the free-stream velocity and boundary-layer thickness.

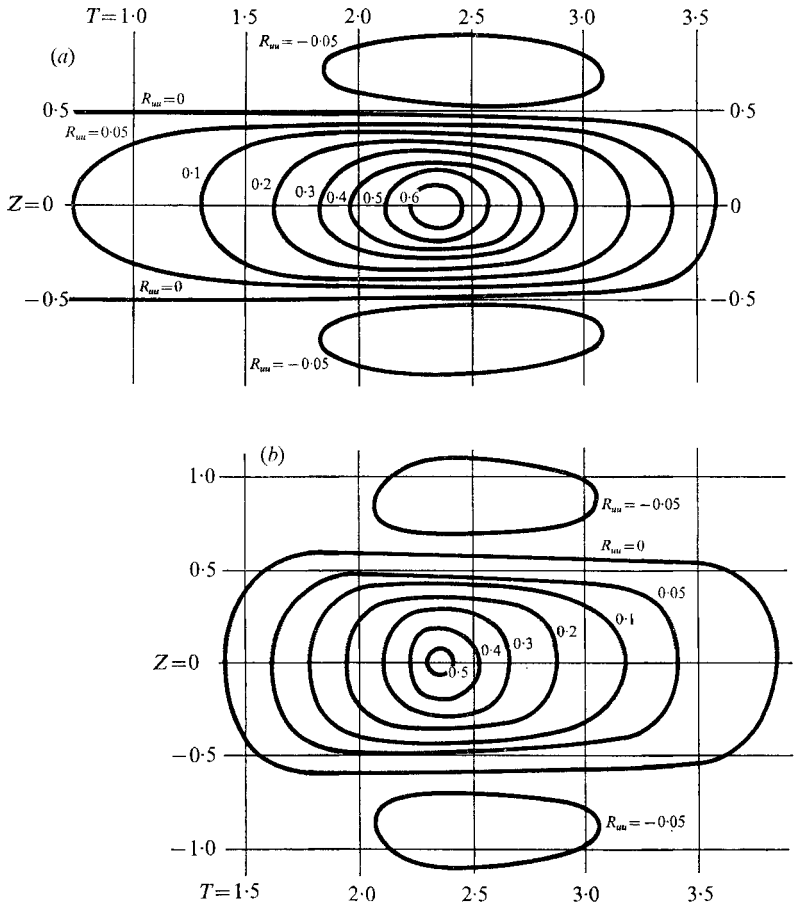

FIGURE 15. Space–time autocorrelation maps of u, $R_{uu}(X_0, 0, Z, T)$. (a) Unaccelerated flow. (b) Accelerated flow.

In all cases in the accelerated flow, the upstream probe was at $x_0 = 973$ cm and $x - x_0 = 43{\cdot}5$ cm was used. The normal distance from the wall was chosen at the half-intermittency point upstream and the downstream probe was positioned to be on the same streamline (ψ_1/ν = constant) as the upstream probe. All of the correlation maps are presented here in the Z, T plane and are compared with the corresponding correlation in the zero pressure gradient flow from Kovasznay, Kibens & Blackwelder (1970). The zero pressure gradient correlations are always shown above the favourable pressure gradient correlations.

$R_{uu}(X_0, 0, Z, T)$ is shown in figure 15, X_0 being the constant streamwise separation. The maximum correlation is slightly less in the accelerated flow and the streamwise elongation of the correlation due to the acceleration is non-existent. The negative lobes flanking the main correlation are still present in the accelerated flow and the spanwise extent is slightly greater. The outstanding feature is the similar shape of the correlation contours under the two different flow conditions which suggests that the acceleration has had little effect on the large eddy structure as reflected by the streamwise velocity.

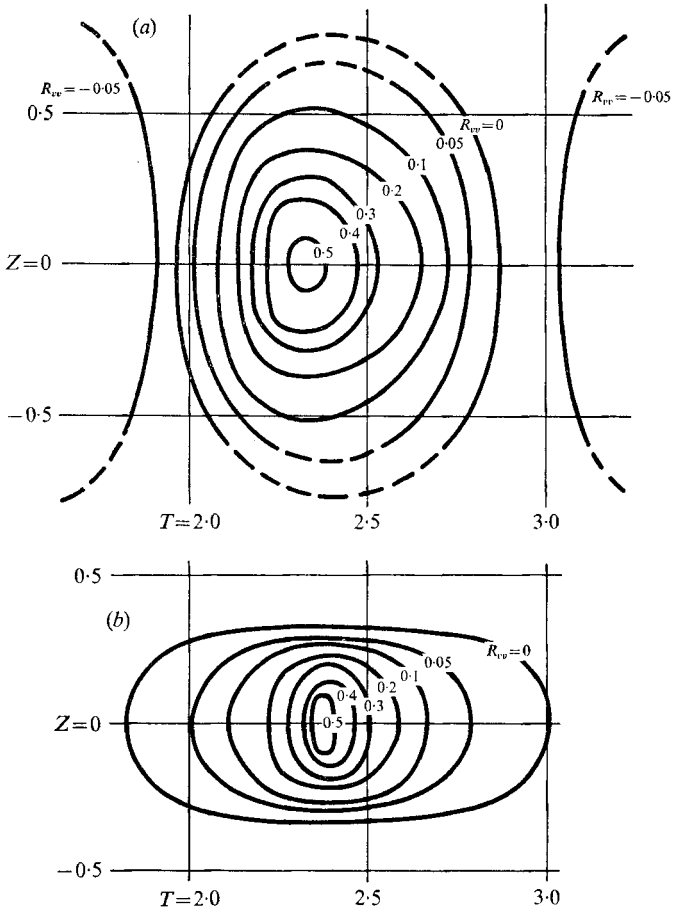

FIGURE 16. Space–time autocorrelation maps of v, $R_{vv}(X_0, 0, Z, T)$. (*a*) Unaccelerated flow. (*b*) Accelerated flow. (——, measured values; – – –, extrapolated values.)

This is not too surprising since Blackwelder & Kovasznay (1972) have shown that in this region of the boundary layer the $1/e$ folding time of the streamwise velocity component equals the time taken to travel approximately seven boundary-layer thicknesses downstream. Evidently, in the early regions of the acceleration the time delay shown in figure 15 is small enough that the acceleration has not been able to significantly alter the streamwise velocity of the eddies.

$R_{vv}(X_0, 0, Z, T)$ is shown in figure 16. The pronounced negative regions found in the unaccelerated flow have disappeared in the accelerated cases, indicating that the anti-symmetrical contribution to the normal velocity component reported by Kovasznay *et al.* (1970) has markedly decreased. At the same time the correlation in the accelerated flow is much narrower in the spanwise direction Z than in the unaccelerated flow. This is somewhat analogous to the results found in the zero pressure gradient case deeper inside the boundary layer (see Kovasznay, Kibens & Blackwelder 1970, figure 19). Thus, even though the acceleration has had little effect on the correlation of the streamwise velocity component, it has had a considerable effect on the normal velocity component. This is unexpected

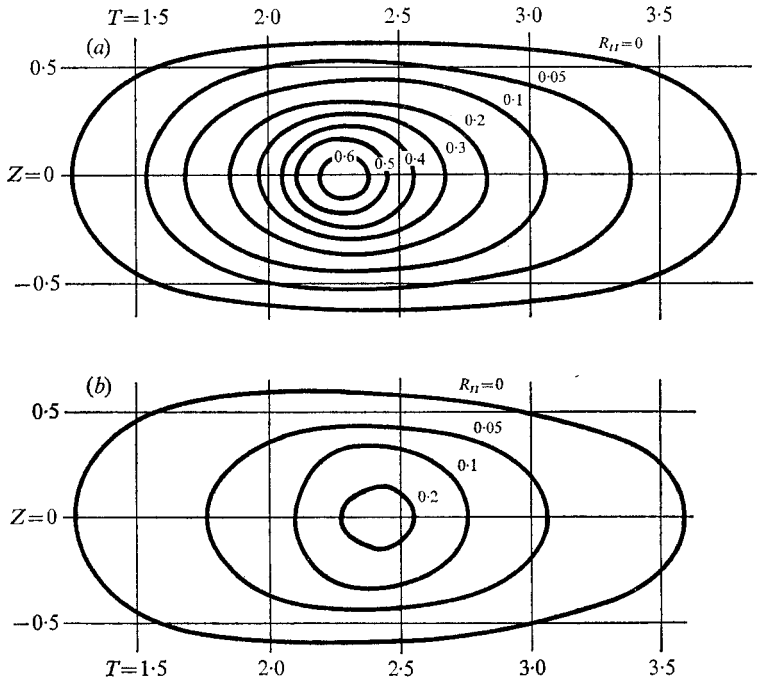

FIGURE 17. Space–time autocorrelation maps of the intermittency function I, $R_{II}(X_0, 0, Z, T)$. (*a*) Unaccelerated flow. (*b*) Accelerated flow.

since the $1/e$ folding time is approximately the same for both velocity components in this region of the boundary layer (Blackwelder & Kovasznay 1972). Evidently the structure of the eddies has been significantly altered in a manner which leaves the correlation of the streamwise velocity component approximately unchanged.

Figure 17 shows the space–time correlation map of the intermittency function I, $R_{II}(X_0, 0, Z, T)$. In both cases the correlation R_{II} was determined according to

$$R_{I_1 I_2} = \frac{\overline{[I_1(x_0, y_0, z_0, t_0) - \gamma_1]\,[I_2(x, y, z, t) - \gamma_2]}}{(I_1 - \gamma_1)' \qquad (I_2 - \gamma_2)'}.$$

In the present case, the intermittency factor is smaller at the downstream location as seen in figure 6; thus the maximum correlation in the accelerated flow is considerably less than in the unaccelerated flow. However, the extent of the $R_{II} = 0$ isocorrelation contour is very similar in the two cases.

The cross-correlations between the normal velocity component and the intermittency function are shown in figures 18 and 19. The $R_{vI}(X_0, 0, Z, T)$ correlations (figure 18) are qualitatively similar, although in the accelerated case no strongly negative regions occur. However, the $R_{Iv}(X_0, 0, Z, T)$ correlations (figure 19) differ considerably. The maximum correlation is less in the accelerated flow and the antisymmetrical component has disappeared completely. The conclusion must be that the antisymmetrical part of the normal velocity component has disappeared completely in the accelerated flow. Furthermore, it has occurred

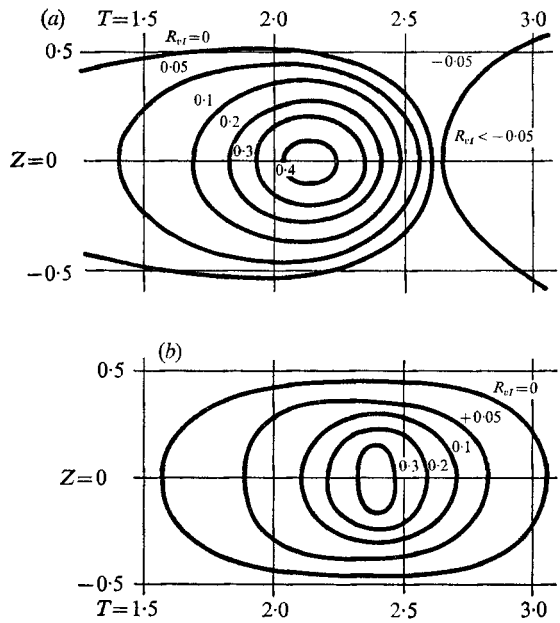

FIGURE 18. Space–time cross-correlation maps of v and I, $R_{vI}(X_0, 0, Z, T)$ (v delayed and I taken at the downstream station). (*a*) Unaccelerated flow. (*b*) Accelerated flow.

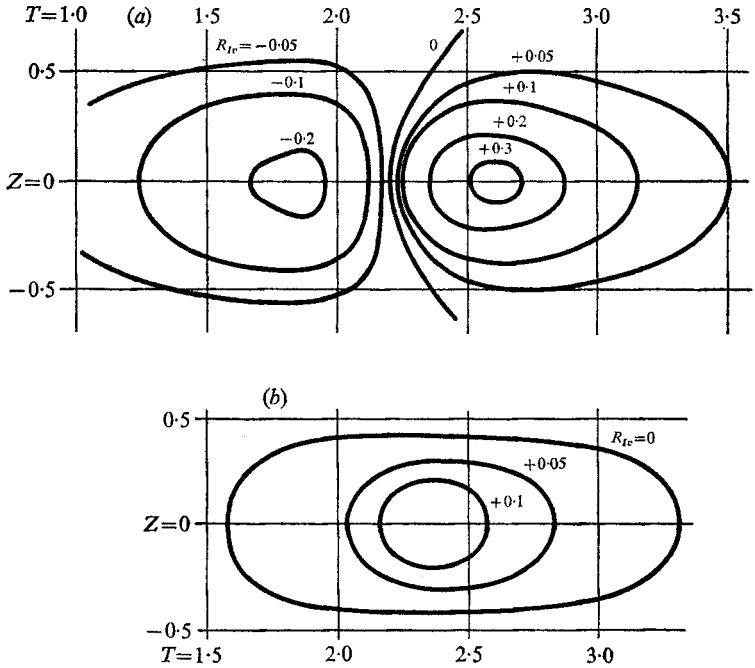

FIGURE 19. Space–time cross-correlation maps of I and v, $R_{Iv}(X_0, 0, Z, T)$ (I delayed and v taken at the downstream station). (*a*) Unaccelerated flow. (*b*) Accelerated flow.

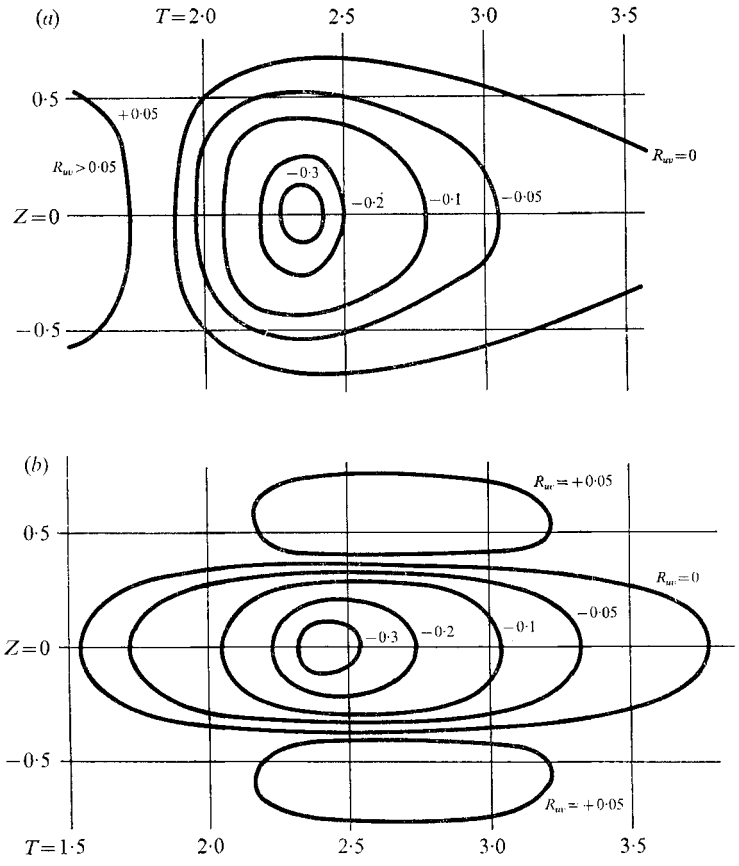

FIGURE 20. Space–time cross-correlation of u and v, $R_{uv}(X_0, 0, Z, T)$ (u delayed and v taken at the downstream station). (*a*) Unaccelerated flow. (*b*) Accelerated flow.

under flow conditions where Kline *et al.* (1967) noticed that the violent eruptions from the buffer layer ceased, suggesting a possible relationship between the two phenomena.

The cross-correlations $R_{uv}(X_0, 0, Z, T)$ are shown in figure 20. Here, u was recorded at the upstream station and delayed before being correlated with values of v taken from the downstream station. Since the antisymmetrical component of v has apparently disappeared in the accelerated flow, the corresponding correlation is approximately symmetrical. The correlation in the accelerated flow spreads less in the Z direction. The positive lobes flanking the main body cannot be compared conclusively because insufficient data were recorded in the zero pressure gradient flow for it to be possible to determine the extent of these positive regions.

The complimentary cross-correlation contours for $R_{vu}(X_0, 0, Z, T)$ are presented in figure 21. Once more the correlation in the accelerated case is more symmetrical in the streamwise (T) direction than in the unaccelerated flow, which agrees with the previous results. Negative lobes possibly exist in the unaccelerated flow but

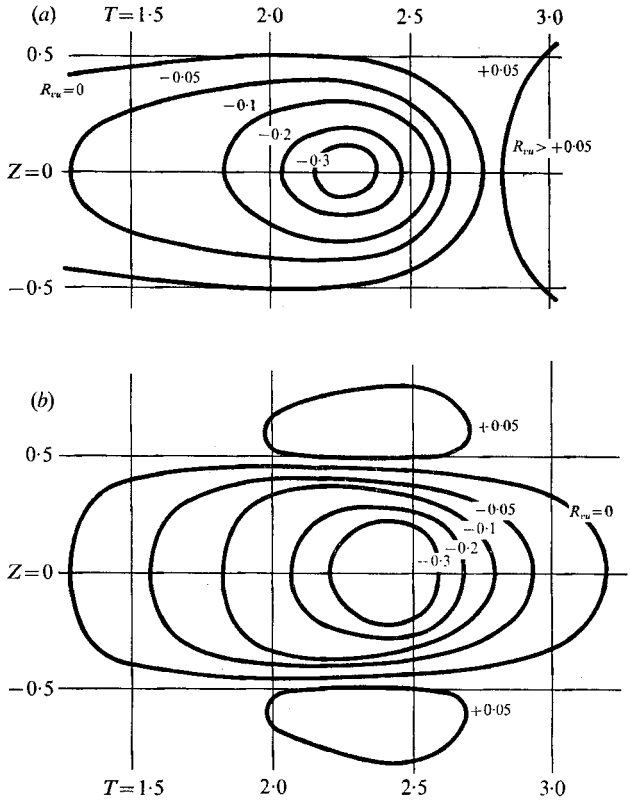

FIGURE 21. Space–time cross-correlation of v and u, $R_{vu}(X_0, 0, Z, T)$ (v delayed and u taken at the downstream station). (*a*) Unaccelerated flow. (*b*) Accelerated flow.

an insufficient amount of data was taken to be able to determine their extent. In figures 20 and 21 the maximum correlations are approximately the same in both the accelerated and unaccelerated cases.

4. Discussion and conclusions

Turbulent boundary layers in strongly favourable pressure gradients develop characteristics which have been classified as 'relaminarization' or 'reverse transition' in the literature. In the experiment presented here, the non-dimensional pressure gradient

$$K = \frac{-\nu}{\rho U_\infty^3}\frac{dp}{dx}$$

exceeded the value which has been reported by various authors as necessary for relaminarization. A large departure from the logarithmic 'law of the wall' was found and the skin friction coefficient at the wall decreased. The mean velocity profile indicated that the thickness of the viscous sublayer increased and the velocity defect in the outer regions decreased. Near the wall the location of the maximum values of the intensity u' moved outwards, which is indicative of the thicker viscous sublayer.

The intermittency factor decreased along the mean streamlines in the favourable pressure gradient flow. After passing through the region of extreme pressure gradient, the intermittency contours indicated that the flow at the wall was only intermittently turbulent between areas of non-turbulent fluid. The total energy of the velocity fluctuations and the Reynolds stress $\overline{uv}$ decreased along the mean streamlines when normalized by the local free-stream velocity $U_\infty(x)$. The absolute value of these quantities, however, remained approximately constant in the outer regions of the boundary layer.

The space–time correlation maps show that the strong antisymmetrical element of the normal velocity component found in the zero pressure gradient by Kovasznay, Kibens & Blackwelder (1970) was no longer present. In the favourable pressure gradient its disappearance roughly occurred in the flow region where Kline *et al.* (1967) noticed that the violent eruptions from the wall region ceased. In other respects, the correlation maps indicate that the large eddy structure was not changed significantly after passing through the strongest part of the favourable pressure gradient.

In terms of the model conjectured by Kovasznay *et al.* (1970) and further elaborated upon by Kovasznay (1970) the following situation seems to be present in the pressure gradient case. After entering the strongly favourable pressure gradient, the eddy eruptions near the wall cease as reported by Kline *et al.* (1967). The cessation of the bursts destroys the constant-stress region as is indicated by the disappearance of the logarithmic mean velocity profile. If these bursts provide most of the momentum exchange between the wall and outer regions, then their stoppage implies that molecular action accounts for more of the momentum exchange, and thus a relatively thicker sublayer must develop.

However, in the outer regions the strongly favourable pressure gradient seems to have almost no effect on the turbulent energy and tangential Reynolds stress. Both the quantities decay very little in absolute terms; i.e. most of their decrease is accounted for by the inflated normalizing quantity $U_\infty(x)$. The most dramatic effect of the pressure gradient in the outer flow field was found in the space–time correlation contours involving the normal velocity component. In all cases the correlations indicated that the antisymmetrical part of the normal velocity component had disappeared. The simultaneous disappearance of this antisymmetrical v component and the turbulent bursts near the wall may perhaps be related but this needs further substantiation.

The authors wish to thank Miss Gail Louise Costigan and Miss Jennie Gill for typing the manuscript. This research was supported by the U.S. Army Research Office, Durham under contract DA-31-124-ARO-d-313 and by the U.S. Air Force through the Office of Scientific Research under contract F44620-69-C-0023.

REFERENCES

Badri Narayanan, M. A. 1968 *J. Fluid Mech.* **31**, 609.

Badri Narayanan, M. A. & Ramjee, V. 1968 *Indian Institute of Science, Bangalore. Rep.* AE 68FMI.

BLACKWELDER, R. F. & KOVASZNAY, L. S. G. 1972 *Phys. Fluids*, to appear.

FIEDLER, H. & HEAD, M. R. 1966 *J. Fluid Mech.* **25**, 719.

KLINE, S. J., REYNOLDS, W. C., SCHRAUB, F. A. & RUNDSTADLER, P. W. 1967 *J. Fluid Mech.* **30**, 741.

KOVASZNAY, L. S. G. 1970 *Ann. Rev. Fluid Mech.* **2**, 95.

KOVASZNAY, L. S. G. & CHEVRAY, R. 1969 *Rev. Sci. Instrum.* **40**, 91.

KOVASZNAY, L. S. G., KIBENS, V. & BLACKWELDER, R. F. 1970 *J. Fluid Mech.* **41**, 283.

KOVASZNAY, L. S. G., MILLER, L. T. & VASUDEVA, B. R. 1963 *Project SQUID, Dept. of Aerospace Engr., University of Virginia Tech. Rep.* JHU-22-P.

MORETTI, P. M. & KAYS, W. M. 1965 *Int. J. Heat Mass Transfer*, **8**, 1187.

PATEL, V. C. & HEAD, M. R. 1968 *J. Fluid Mech.* **34**, 371.

STERNBERG, J. 1954 *U.S. Army Bal. Res. Lab. Rep.* no. 906.

STEWART, R. W. 1956 *J. Fluid Mech.* **11**, 593.